# CHAPTER IV
RESULTS AND DISCUSSION

4.1 Photocatalyst Characterizations

4.1.1 TG-DTA Results

The TG-DTA curves were used to study the thermal decomposition behavior of the synthesized dried photocatalysts and to obtain their suitable calcination temperatures. Figure 4.1 exemplifies the TG-DTA curves of the dried pure TiO_2 and $0.97TiO_2$-$0.03SiO_2$ mixed oxide gels. The DTA curves show three main exothermic regions, as also summarized in Table 4.1. The first exothermic peak, with its position lower than 150 °C, is attributed to the removal of physisorbed water molecules. The second exothermic peak, with its position between 150 and 320 °C, is attributed to the burnout of the LAHC surfactant molecules. The third exothermic peak between 320 and 500 °C corresponds to the crystallization process of the photocatalysts, as well as the removal of organic remnants and chemisorbed water molecules (Hague et al., 1994). The TG curves reveal that the weight losses ended at a temperature of approximately 500 °C for both dried photocatalysts. Therefore, the calcination temperature of 500 °C was sufficient for both the complete surfactant removal and the photocatalyst crystallization process. Therefore, the calcination temperature in the range of 500 and 800 °C was used to investigate its effect on physicochemical properties and consequent photocatalytic hydrogen production activity of all the synthesized photocatalysts.
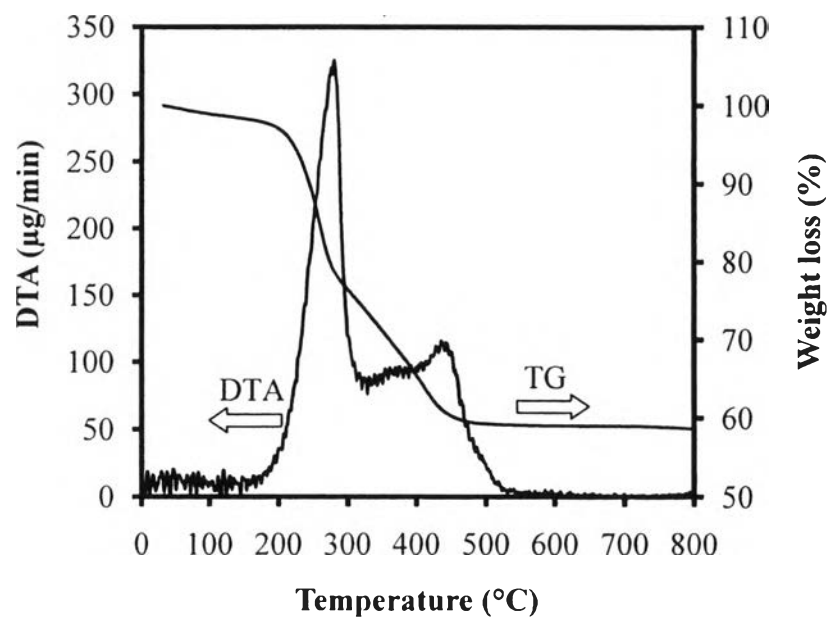
(a)
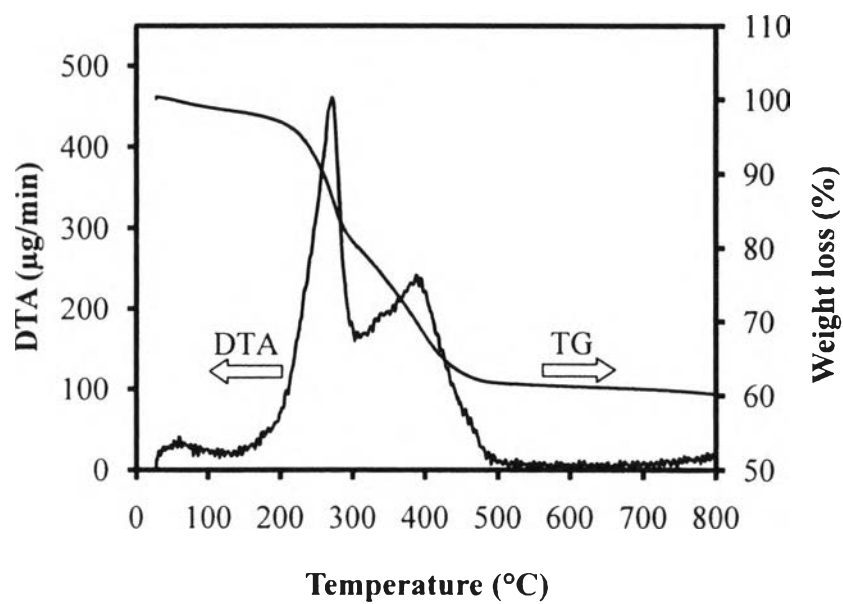
(b)

Figure 4.1 TG-DTA curves of the dried synthesized photocatalysts: (a) pure TiO_2 and (b) $0.97TiO_2$·$0.03SiO_2$ mixed oxide.

Table 4.1 Thermal decomposition results of the dried synthesized pure TiO_2 and $0.97TiO_2$-$0.03SiO_2$ mixed oxide photocatalysts from TG-DTG analysis

Photocatalyst	Position of exothermic peak (°C)			Corresponding weight loss (wt.%)			
	1st region	2nd region	3rd region	1st region	2nd region	3rd region	Total
TiO_2	30-150	150-320	320-500	1.80	19.51	17.00	38.31
$0.97TiO_2$-$0.03SiO_2$	30-150	150-320	320-500	1.72	24.03	14.99	40.74

4.1.2 N_2 Adsorption-Desorption Results

The N_2 adsorption-desorption analysis was used to verify the mesoporosity of the TiO_2-SiO_2 mixed oxide photocatalysts with different TiO_2-to-SiO_2 molar ratios. The shape of the isotherms exhibits the characteristic behavior of the structure of powder, which is composed of an assembly of particles with uniform pore opening. The N_2 adsorption-desorption isotherms of the pure TiO_2, $0.97TiO_2$-$0.03SiO_2$ mixed oxide, and Pt-loaded and bimetallic Pt-Au-loaded $0.97TiO_2$-$0.03SiO_2$ mixed oxide photocatalysts calcined at 500 °C are exemplified in Figures 4.2-4.4. All of the samples exhibit typical IUPAC type IV pattern with H2-type hysteresis loop, which is the major characteristic of a mesoporous material (mesoporous size between 2 and 50 nm) according to the classification of IUPAC (Rouquerol *et al.*, 1999). A sharp increase in the adsorption curves at a high relative pressure (P/P_0) implies a capillary condensation of N_2 molecules inside the mesopores, implying the well-uniform mesopores and narrow pore size distributions since the P/P_0 position of the inflection point is directly related to the pore dimension. The insets of Figures 4.2-4.4 show the pore size distributions calculated from the desorption branch of the isotherms by the DH method. The pure TiO_2 and $0.97TiO_2$-

$0.03SiO_2$ mixed oxide photocatalysts without and with 1.25 wt.% Pt loading and bimetallic 0.75 wt.% Pt-0.75 wt.% Au loading possess quite narrow pore size distributions entirely locating in the mesoporous region (between 2 and 50 nm), implying a good quality of the samples. Table 4.2 shows the textural properties from the N_2 adsorption-desorption analysis of the pure TiO_2 and TiO_2-SiO_2 mixed oxide photocatalysts calcined at various temperatures. It is clearly observed that at the calcination temperature of 500 °C, the incorporation of SiO_2 into TiO_2 resulted in an increase in specific surface area, as can be clearly seen from the results that for example, by incorporating 3 mol% SiO_2 into TiO_2 to obtain the $0.97TiO_2$-$0.03SiO_2$ mixed oxide (which exhibited the highest photocatalytic activity among the mixed oxide series, as shown later), the specific surface area increased from 55.3 to 161.8 $m^2 \cdot g^{-1}$. The presence of this second metal oxide with appropriate amounts could retard crystallization process and affect the growth of bulk material, which was confirmed by the XRD analysis in the next section, resulting in higher specific surface areas of the mixed oxide photocatalysts (Schattka *et al.*, 2002). In case of increasing calcination temperature from 500 to 800 °C, it can be seen from Table 4.2 that the 3 mol% SiO_2-incorporated TiO_2 (i.e. $0.97TiO_2$-$0.03SiO_2$ mixed oxide) could retain its specific surface area much more than the pure TiO_2 at high calcination temperatures. The specific surface area of the pure TiO_2 was smaller and decreased more quickly from 55.3 to 3.5 $m^2 \cdot g^{-1}$ when increasing calcination temperature from 500 to 800 °C as compared to the $0.97TiO_2$-$0.03SiO_2$ mixed oxide, of which its specific surface area decreased from 161.8 $m^2 \cdot g^{-1}$ to 73.5 $m^2 \cdot g^{-1}$ when increasing calcination temperature from 500 to 800 °C. As expected, the observed loss in the specific surface area with increasing calcination temperature for both photocatalysts is possibly because of the pore collapse due to both the destruction of walls separating the mesopores upon the crystallization and the grain growth of the photocatalyst crystallites, which consequently led to an increase in the mean mesopore diameter with a simultaneous decrease in the total pore volume (Table 4.2).
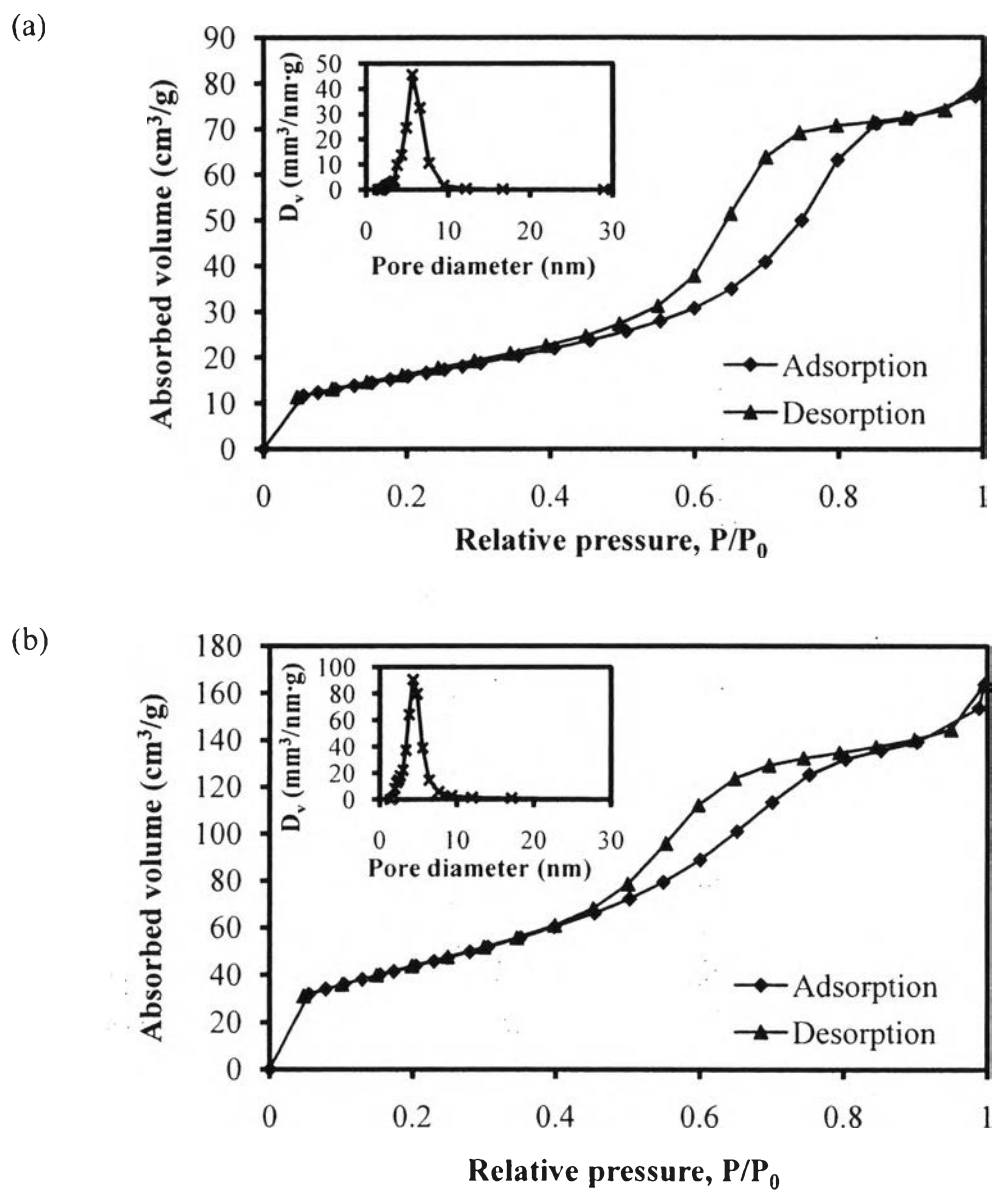
(a)

(b)

Figure 4.2 N_2 adsorption-desorption isotherms and pore size distributions (inset) of the synthesized mesoporous-assembled photocatalysts calcined at 500 °C: (a) pure TiO_2 and (b) $0.97TiO_2$-$0.03SiO_2$ mixed oxide.
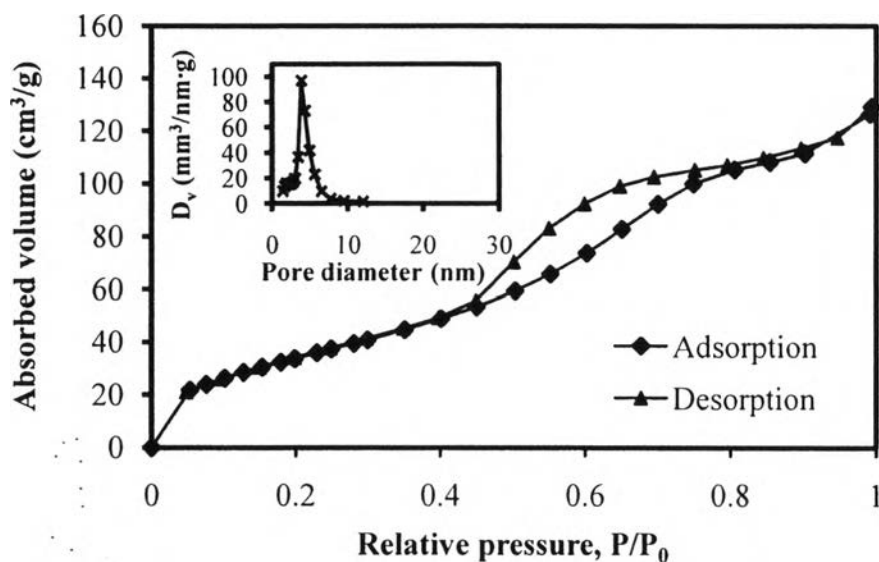
Figure 4.3 N_2 adsorption-desorption isotherms and pore size distribution (inset) of the synthesized 1.25 wt.% Pt-loaded mesoporous-assembled $0.97TiO_2$-$0.03SiO_2$ mixed oxide photocatalyst calcined at 500 °C.
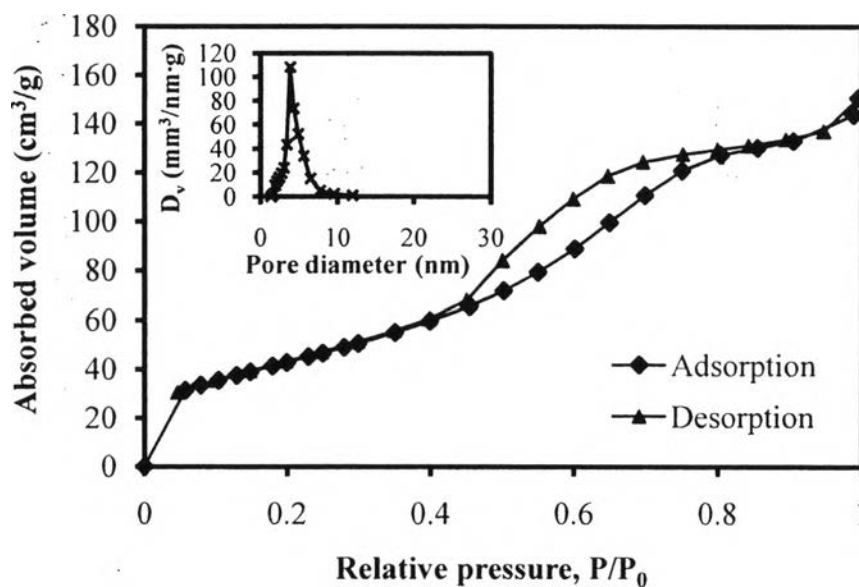

Figure 4.4 N_2 adsorption-desorption isotherms and pore size distribution (inset) of the synthesized 0.75 wt.% Pt-0.75 wt.% Au-loaded mesoporous-assembled $0.97TiO_2$-$0.03SiO_2$ mixed oxide photocatalyst calcined at 500 °C.

Table 4.2   N$_2$ adsorption-desorption results of the synthesized mesoporous-assembled pure TiO$_2$ and TiO$_2$-SiO$_2$ mixed oxide photocatalysts calcined at various temperatures

Photocatalyst	Calcination temperature (°C)	Specific surface area (m^2·g^{-1})	Mean mesopore diameter (nm)	Total pore volume (cm^3·g^{-1})
Pure TiO$_2$	500	55.3	5.60	0.114
0.99TiO$_2$-0.01SiO$_2$	500	122.0	4.92	0.203
0.97TiO$_2$-0.03SiO$_2$	500	161.8	4.30	0.240
0.95TiO$_2$-0.05SiO$_2$	500	180.6	4.31	0.256
0.93TiO$_2$-0.07SiO$_2$	500	186.4	3.83	0.282
Pure TiO$_2$	500	55.3	5.60	0.114
	600	12.0	3.81	0.035
	700	4.4	_[a]	_[a]
	800	3.5	_[a]	_[a]
0.97TiO$_2$-0.03SiO$_2$	500	161.8	4.30	0.240
	600	122.7	5.62	0.208
	700	70.7	6.58	0.150
	800	73.5	6.56	0.161

[a] N$_2$ adsorption-desorption isotherms correspond to IUPAC type II pattern.

Table 4.3 shows the summary of textural properties of the synthesized Pt-loaded mesoporous-assembled $0.97TiO_2$-$0.03SiO_2$ mixed oxide photocatalysts calcined at 500 °C. The results show that the specific surface area, mean mesopore diameter, and total pore volume of the Pt-loaded $0.97TiO_2$-$0.03SiO_2$ mixed oxides moderately decreased with increasing Pt loading. The decreases in the specific surface area, mean mesopore diameter, and total pore volume when the Pt particles were deposited on the mixed oxide support can be possibly attributed to the blockage of a small portion of mesopores of the mixed oxide support by the Pt particles deposited inside the mesoporous-assembled structure. The similar tendencies of such decreases could also be deserved for the synthesized bimetallic Pt-Au-loaded mesoporous-assembled $0.97TiO_2$-$0.03SiO_2$ mixed oxide photocatalysts calcined at 500 °C, as shown in Table 4.4. However, it was interestingly found that the specific surface area of the 0.75 wt.% Pt-0.75 wt.% Au-loaded $0.97TiO_2$-$0.03SiO_2$ mixed oxide was higher than the other photocatalysts with bimetallic Pt-Au loading.

Table 4.3 N_2 adsorption-desorption results of the synthesized Pt-loaded mesoporous-assembled $0.97TiO_2$-$0.03SiO_2$ mixed oxide photocatalysts calcined at 500 °C

Pt loading (wt.%)	Specific surface area $(m^2 \cdot g^{-1})$	Mean mesopore diameter (nm)	Total pore volume $(cm^3 \cdot g^{-1})$
0	161.8	4.30	0.240
0.5	137.5	4.30	0.204
0.75	141.2	3.83	0.200
1	142.8	4.31	0.202
1.25	133.1	3.82	0.195
1.5	129.4	3.82	0.193

Table 4.4 N$_2$ adsorption-desorption results of the synthesized bimetallic Pt-Au-loaded mesoporous-assembled 0.97TiO$_2$-0.03SiO$_2$ mixed oxide photocatalysts calcined at 500 °C

Pt loading (wt.%)	Au loading (wt.%)	Specific surface area (m^2·g^{-1})	Mean mesopore diameter (nm)	Total pore volume (cm^3·g^{-1})
0	0	161.8	4.30	0.240
1.5	0	129.4	3.82	0.193
1.25	0.25	146.1	3.81	0.211
1	0.5	137.5	3.82	0.177
0.75	0.75	160.0	3.83	0.222
0.5	1	145.6	3.81	0.191
0.25	1.25	150.4	3.83	0.197
0	1.5	158.9	3.83	0.227

4.1.3 XRD Results

The XRD patterns of the mesoporous-assembled TiO$_2$-SiO$_2$ mixed oxide photocatalysts with different TiO$_2$-to-SiO$_2$ molar ratios calcined at 500 °C are shown in Figure 4.5. The XRD pattern of the pure TiO$_2$ shows crystalline structure of the pure anatase phase. The dominant peaks at 2θ of about 25.2°, 37.9°, 48.3°, 53.8°, and 55.0° which represent the indices of (101), (103), (200), (105), and (211) planes, respectively (Smith, 1960), correspond to the crystalline anatase TiO$_2$ phase. The mixed oxide samples with TiO$_2$-to-SiO$_2$ molar ratios of 99:1, 97:3, 95:5 and 93:7 also show diffraction peaks attributed to the anatase TiO$_2$. Although the SiO$_2$ was incorporated up to 7 mol%, the crystalline structure of the mixed oxides was still the anatase TiO$_2$. Hence, the incorporated SiO$_2$ at such low contents did not significantly affect the crystalline structure of the synthesized TiO$_2$-SiO$_2$ mixed oxide photocatalysts. However, the peak intensities gradually decreased with increasing SiO$_2$ content possibly because a further increase in the SiO$_2$ content more greatly inhibited the crystallization process of the TiO$_2$.
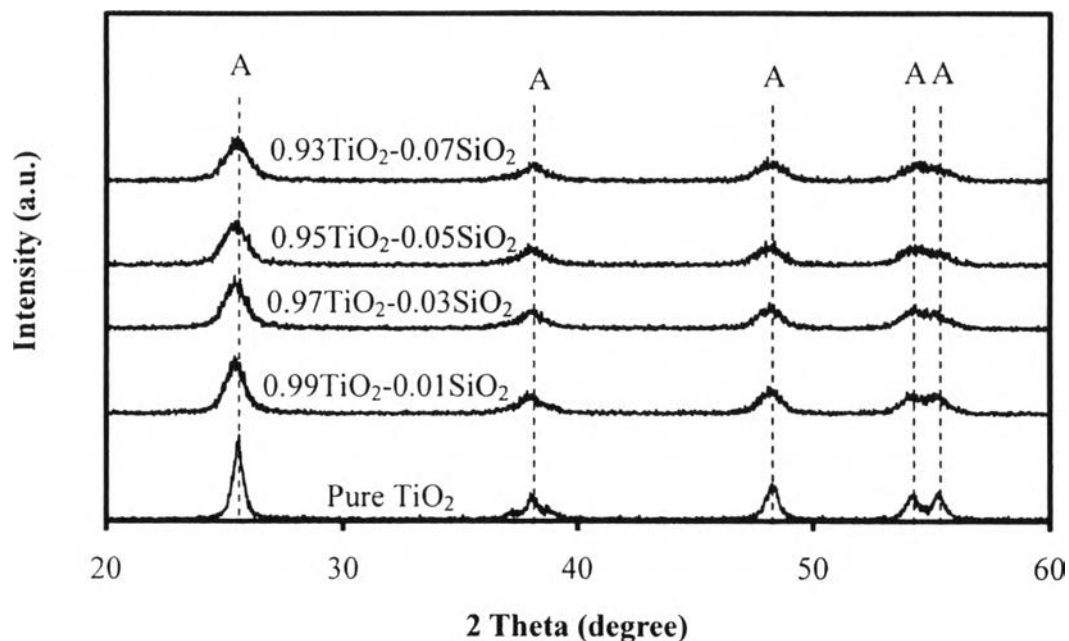
Figure 4.5 XRD patterns of the synthesized mesoporous-assembled pure TiO_2 and TiO_2-SiO_2 mixed oxide photocatalysts calcined at 500 °C (A = Anatase TiO_2).

Figure 4.6 shows the XRD patterns of the synthesized mesoporous-assembled pure TiO_2 and $0.97TiO_2$-$0.03SiO_2$ mixed oxide photocatalysts calcined at various temperatures between 500 and 800 °C. As shown in Figure 4.6(a), the XRD pattern of the pure TiO_2 photocatalyst calcined at 500 °C shows crystalline structure of the pure anatase phase, as mentioned above. The pure TiO_2 photocatalyst underwent the anatase-to-rutile phase transformation beginning at 600 °C, resulting in the combination of the anatase and rutile phases. The occurrence of the dominant peaks at 2θ of about 27.5°, 36.0°, 39.0°, 41.2°, 44.1°, 54.2°, and 56.7°, which correspond to the indices of (110), (101), (200), (111), (210), (211), and (220) planes, respectively (Smith, 1960), indicates the presence of the rutile phase. The rutile ratio (W_R) in terms of its weight fraction was estimated from the XRD intensity data by using Eq. (4.1) (Spurr and Myers, 1957)

$$W_R = [1 + 0.8I_A/I_R]^{-1} \qquad (4.1)$$

where I_A and I_R represent the integrated intensities of anatase (101) and rutile (110) diffraction peaks, respectively. All calculated values of the rutile ratio (W_R) are presented in Table 4.5. A steadily increased phase transformation was observed until

the pure TiO_2 photocatalyst contained the pure rutile phase after calcined at 800 °C. However, this phase transformation behavior did not occur for the $0.97TiO_2$-$0.03SiO_2$ mixed oxide photocatalyst. Figure 4.6(b) reveals that the incorporation of 3 mol% SiO_2 delayed the phase transformation of TiO_2 from the meta-stable anatase phase to the themally-stable rutile phase (Lin et al., 1994), since the mixed oxide photocatalyst sample displays the dominant XRD peaks corresponding to only the pure anatase phase even when it was calcined at as high as 800 °C.

The crystallite size of the photocatalysts was calculated from the line broadening of the most preferentially oriented diffraction peak of each crystalline phase according to the Sherrer equation (Cullity, 1978) (Eq. 4.2):

$$L = \frac{k}{\beta \cos(\theta)} \tag{4.2}$$

where L is the crystallite size, k is the Sherrer constant usually taken as 0.89, λ is the wavelength of the X-ray radiation (0.15418 nm for Cu Kα), β is the full width at half maximum (FWHM) of the diffraction peak measured at 2θ, and θ is the diffraction angle. The crystallite sizes of the synthesized mesoporous-assembled pure TiO_2 and TiO_2-SiO_2 mixed oxide photocatalysts are given in Table 4.5. The results reveal that the incorporation of SiO_2 led to the decrease in crystallite size due to the role of SiO_2 in retarding the growth of the TiO_2 crystals. With increasing calcination temperature, a larger crystallite size was observed for both the pure TiO_2 and $0.97TiO_2$-$0.03SiO_2$ mixed oxide photocatalysts due to the grain growth induced by an increased temperature.

(a)

(b)

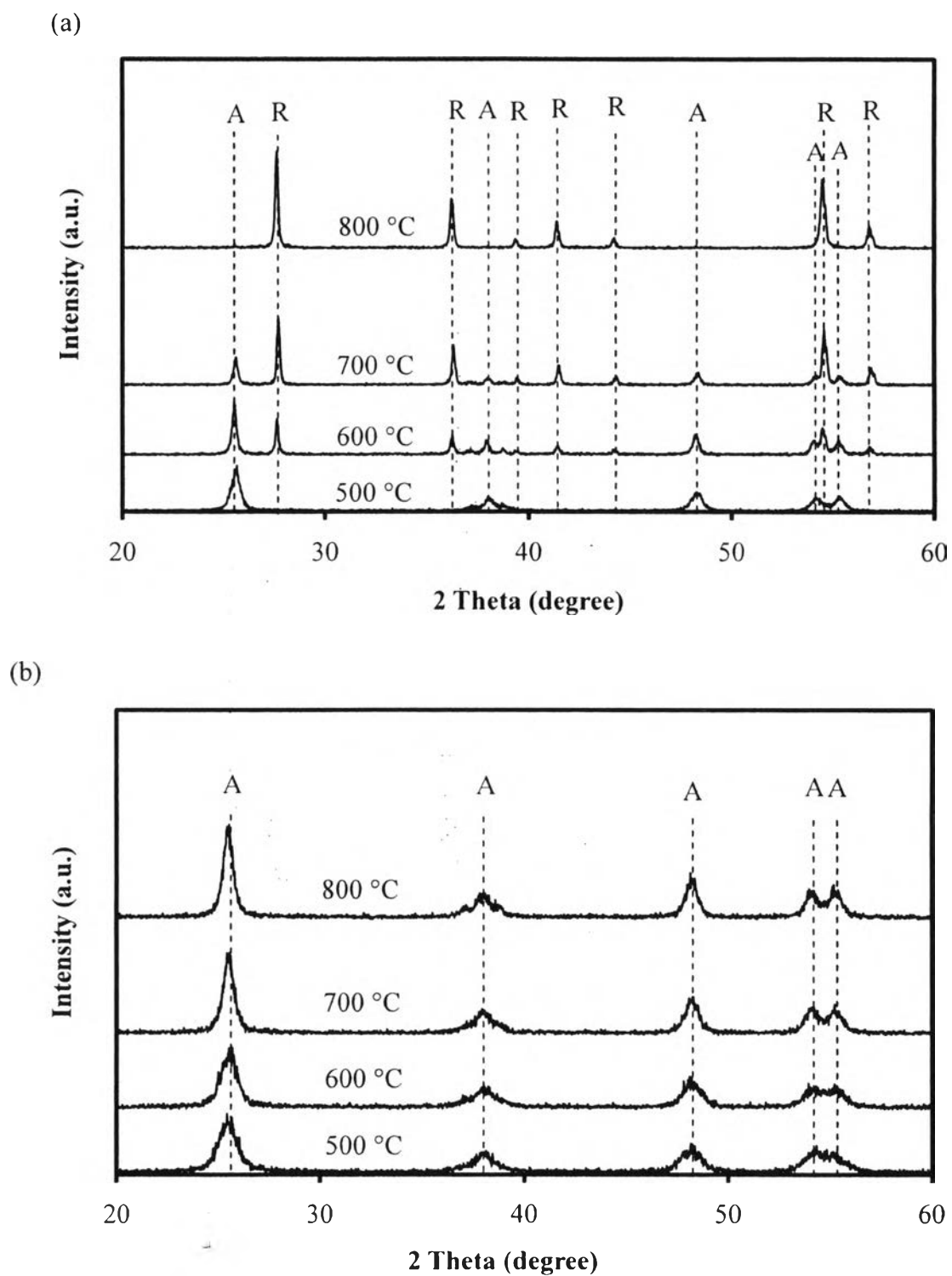**Figure 4.6** XRD patterns of the synthesized mesoporous-assembled photocatalysts calcined at 500–800 °C: (a) pure TiO_2 and (b) $0.97TiO_2$-$0.03SiO_2$ mixed oxide (A = Anatase TiO_2, R = Rutile TiO_2).

Table 4.5 XRD results of the synthesized mesoporous-assembled pure TiO_2 and TiO_2-SiO_2 mixed oxide photocatalysts calcined at various temperatures

Photocatalyst	Calcination temperature (°C)	Phase from XRD pattern	Rutile ratio	Crystallite size (nm)	
				Anatase (101)	Rutile (110)
Pure TiO_2	500	Anatase	-	15.62	-
$0.99TiO_2$-$0.01SiO_2$	500	Anatase	-	8.62	-
$0.97TiO_2$-$0.03SiO_2$	500	Anatase	-	7.41	-
$0.95TiO_2$-$0.05SiO_2$	500	Anatase	-	6.40	-
$0.93TiO_2$-$0.07SiO_2$	500	Anatase	-	6.52	-
Pure TiO_2	500	Anatase	-	15.62	-
	600	Anatase +Rutile	0.44	28.53	36.31
	700	Anatase +Rutile	0.74	29.75	36.63
	800	Rutile	1	-	36.63
$0.97TiO_2$-$0.03SiO_2$	500	Anatase	-	7.41	-
	600	Anatase	-	7.84	-
	700	Anatase	-	13.02	-
	800	Anatase	-	13.78	-

The XRD patterns of the synthesized Pt-loaded mesoporous-assembled $0.97TiO_2$-$0.03SiO_2$ mixed oxide photocatalysts calcined at 500 °C are shown in Figure 4.7. All the diffraction peaks corresponded to the crystalline structure of the anatase TiO_2. The presence of Pt in the photocatalysts could be observed at high Pt loadings by a diffraction peak at 2θ of 39.8°, which corresponds to the index of Pt (111) plane; however, the peak intensity was quite weak possibly because of its low content and high dispersion. Moreover, Figure 4.8 shows the XRD patterns of the synthesized bimetallic Pt-Au-loaded mesoporous-assembled $0.97TiO_2$-$0.03SiO_2$ mixed oxide photocatalysts calcined at 500 °C. The anatase TiO_2 diffraction peaks were also mainly observed, where the diffraction peak at 2θ of 44.3° representing the index of Au (200) plane could be seen at high Au loadings, similar to the Pt peak at high Pt loadings. For both the Pt-loaded and bimetallic Pt-Au-loaded $0.97TiO_2$-$0.03SiO_2$ mixed oxide photocatalysts, the crystallite size was insignificantly affected by the metal loadings possibly due to their relatively low loading contents, as shown in Tables 4.6 and 4.7.
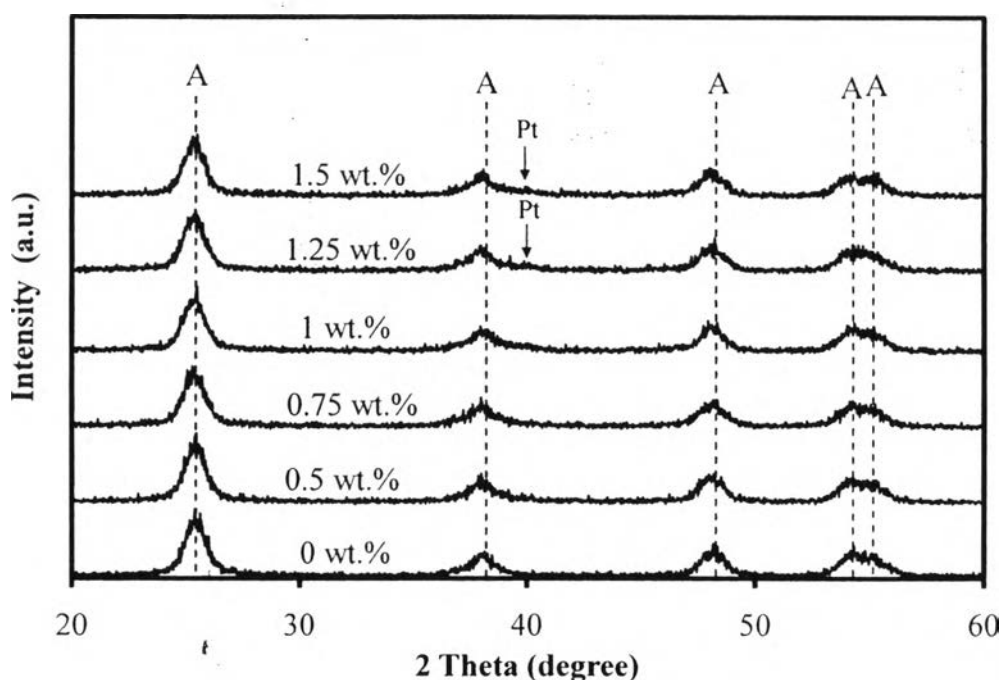

Figure 4.7 XRD patterns of the synthesized Pt-loaded mesoporous-assembled $0.97TiO_2$-$0.03SiO_2$ mixed oxide photocatalysts calcined at 500 °C (A = Anatase TiO_2).
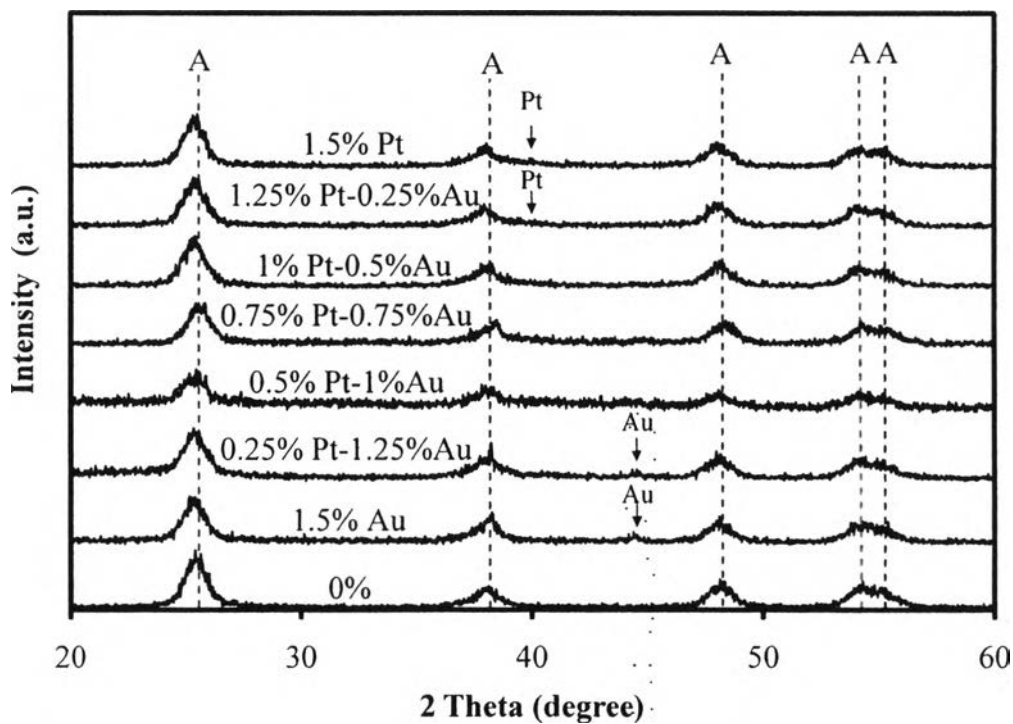
Figure 4.8 XRD patterns of the synthesized bimetallic Pt-Au-loaded mesoporous-assembled $0.97TiO_2$-$0.03SiO_2$ mixed oxide photocatalysts calcined at 500 °C (A = Anatase TiO_2).

Table 4.6 XRD results of the synthesized Pt-loaded mesoporous-assembled $0.97TiO_2$-$0.03SiO_2$ mixed oxide photocatalysts calcined at 500 °C

Pt loading (wt.%)	Anatase (101) crystallite size (nm)
0	7.41
0.5	7.67
0.75	7.4
1	6.96
1.25	7.29
1.5	7.34

Table 4.7 XRD results of the synthesized bimetallic Pt-Au-loaded mesoporous-assembled $0.97TiO_2$-$0.03SiO_2$ mixed oxide photocatalysts calcined at 500 °C

Pt loading (wt.%)	Au loading (wt.%)	Anatase (101) crystallite size (nm)
1.5	0	7.34
1.25	0.25	7.20
1	0.5	7.39
0.75	0.75	7.47
0.5	1	6.83
0.25	1.25	7.20
0	1.5	7.50

4.1.4 UV-Visible Spectroscopy Results

UV-visible spectroscopy was used to examine the light absorption ability of the synthesized mesoporous-assembled TiO_2-SiO_2 mixed oxide photocatalysts without and with Pt and/or Au loading, as well as that of Eosin Y (E.Y.) solution, which was used as a sensitizer for the photocatalytic hydrogen production in this work. Figure 4.9 shows the UV-visible spectra of the mesoporous-assembled TiO_2-SiO_2 mixed oxide photocatalysts with different TiO_2-to-SiO_2 molar ratios calcined at 500 °C. It is clearly seen that the absorption band of the synthesized mesoporous-assembled TiO_2-SiO_2 mixed oxide photocatalysts was mainly in the UV light region in the range of low wavelength up to 400 nm. The band gap energy (E_g, eV) was determined by extrapolating the absorption onset of the rising part to x-axis (λ_g, nm) of the plots, as shown by dashed line in Figure 4.9, and calculated by Eq. (4.3):

$$E_g = 1240 / \lambda_g \tag{4.3}$$

where λ_g is the wavelength (nm) of the exciting light. The results of absorption onset wavelength and corresponding band gap energy of all the photocatalysts obtained from the UV-visible spectra are summarized in Table 4.8. With increasing SiO_2

content in the mixed oxide photocatalysts, the band gap energy gradually increased from 3.22 (λ_g = 385 nm) for the pure TiO_2 to 3.32 eV (λ_g = 373 nm) for the 0.97TiO_2-0.03SiO_2 mixed oxide. The shift of the absorption onset edge in the TiO_2-SiO_2 mixed oxides can be attributed to quantum-size effect for smaller crystallites (Andrulevicius *et al.*, 2007), since it is known that TiO_2 crystallization and its crystallite growth are inhibited in the presence of SiO_2, as shown above in the XRD results. In case of increasing calcination temperature from 500 to 800 °C for the 0.97TiO_2-0.03SiO_2 mixed oxide as shown in Figure 4.10, the shift of the absorption onset edge toward a longer wavelength could be observed. As also included in Table 4.8, the band gap energy of the 0.97TiO_2-0.03SiO_2 mixed oxide decreased from 3.26 eV (λ_g = 380 nm) at the calcination temperature of 500 °C to 3.20 eV (λ_g = 388 nm) at the calcination temperature of 800 °C. This shift is normally due to the narrowing of the band gap energy, which results in a lower energy required for electrons to be excited from the valence band to conduction band (Sreethawong *et al.*, 2009). Interestingly, the band gap energy of the 0.97TiO_2-0.03SiO_2 mixed oxide was maintained at the anatase-TiO_2 band gap energy, even though it was calcined at as high as 800 °C. The comparative results of UV-visible spectra of the mesoporous-assembled 0.97TiO_2-0.03SiO_2 mixed oxide photocatalysts calcined at 500 °C without and with 1.25 wt.% Pt and bimetallic 0.75 wt.% Pt-0.75 wt.% Au loadings are exemplified in Figure 4.11. The band gap energies of the 1.25 wt.% Pt-loaded mesoporous-assembled 0.97TiO_2-0.03SiO_2 and the 0.75 wt.% Pt-0.75 wt.% Au-loaded 0.97TiO_2-0.03SiO_2 mixed oxide photocatalysts were quite the same at approximately 3.33 eV (λ_g ~ 372 nm) and 3.36 eV (λ_g ~ 369 nm), respectively (Table 4.8), which were almost similar to that of the host 0.97TiO_2-0.03SiO_2 mixed oxide photocatalyst. However, the Pt- and bimetallic Pt-Au-loaded samples showed more visible light absorption ability than the unloaded sample. It can also be clearly observed that most of the TiO_2-SiO_2 mixed oxide photocatalysts could absorb only UV light of wavelength shorter than 420 nm. Therefore, in order to confirm that Eosin Y (E.Y.) is the visible light-responding sensitizer, its UV-visible spectrum was also measured, as shown in Figure 4.12. It is clear that E.Y. could mainly absorb the visible light with the maximum absorption centered at 516 nm. This absorption feature strongly suggests that the sensitizer can

be activated by the visible light for the sensitized photocatalytic hydrogen production system in this work.
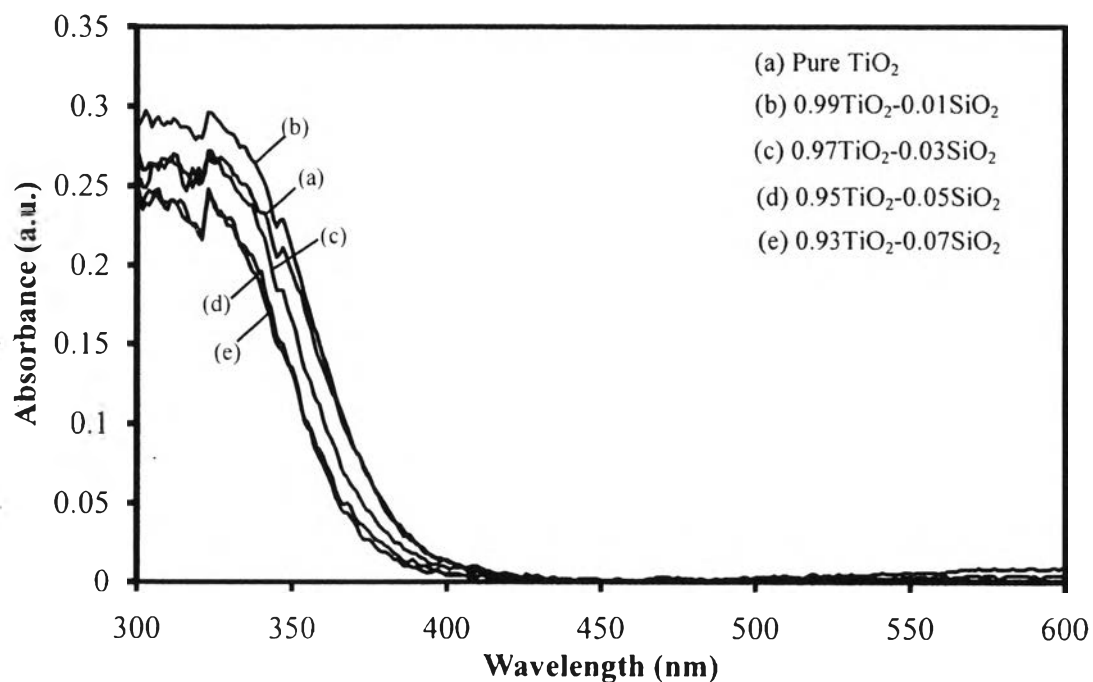

Figure 4.9 UV-visible spectra of the synthesized mesoporous-assembled photocatalysts calcined at 500 °C: (a) pure TiO_2 and (b)-(e) TiO_2-SiO_2 mixed oxide.
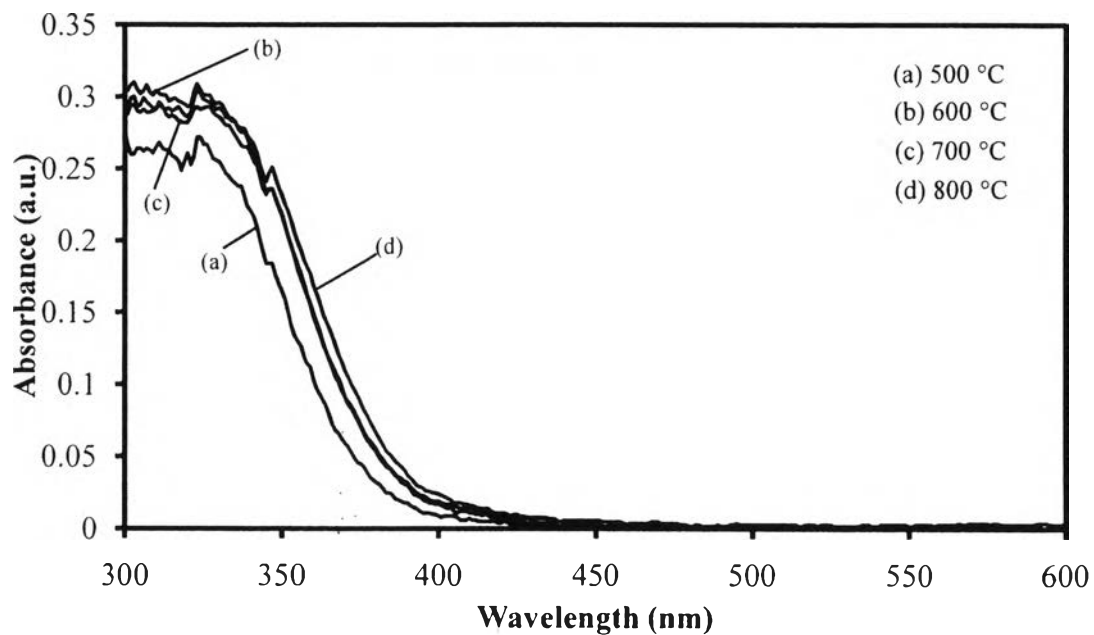
Figure 4.10 UV-visible spectra of the synthesized mesoporous-assembled 0.975TiO₂-0.03SiO₂ mixed oxide photocatalysts calcined at various temperatures.

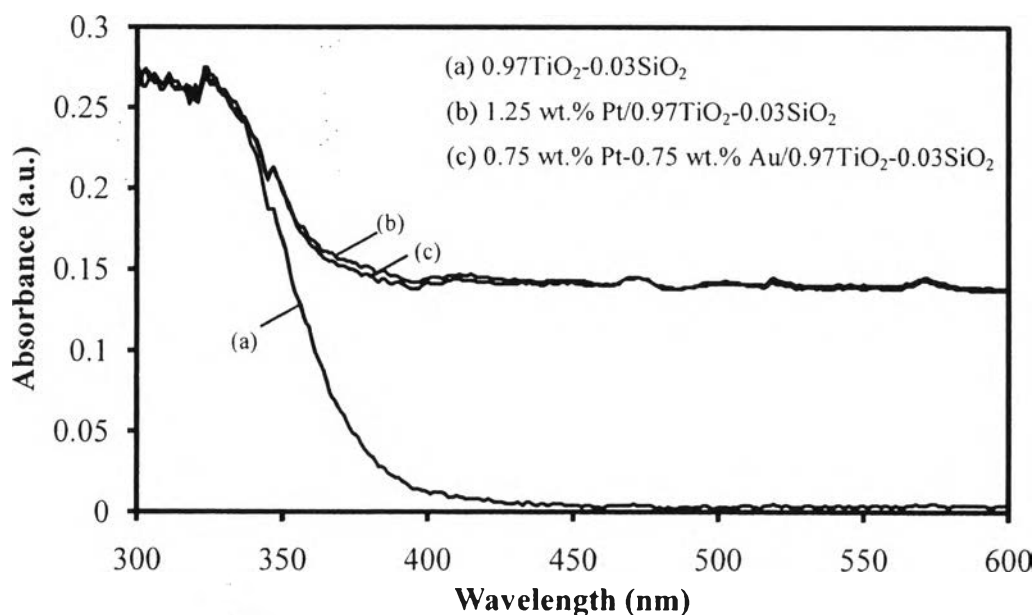**Figure 4.11** UV-visible spectra of the synthesized mesoporous-assembled photocatalysts calcined at 500 °C: (a) 0.97TiO₂-0.03SiO₂ mixed oxide, (b) 1.25 wt.% Pt-loaded 0.975TiO₂-0.03SiO₂ mixed oxide, and (c) the 0.75 wt.% Pt-0.75 wt.% Au-loaded 0.97TiO₂-0.03SiO₂ mixed oxide.

Table 4.8   Absorption onset wavelength and band gap energy results of the synthesized mesoporous-assembled TiO_2-SiO_2 mixed oxide photocatalysts without and with metal loadings and calcined at various temperatures

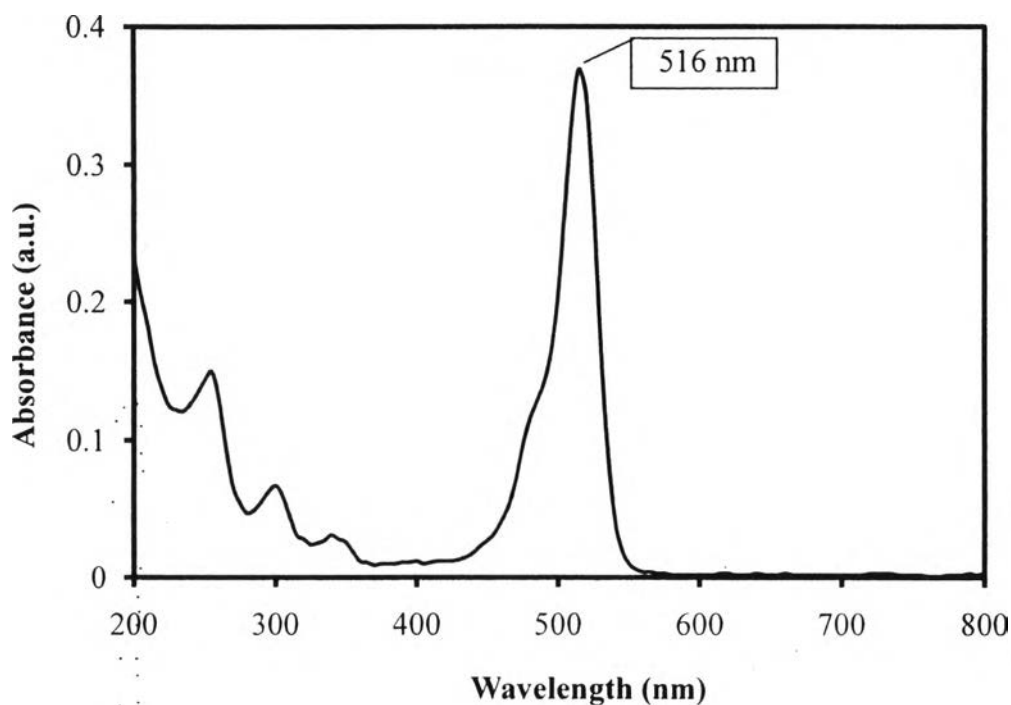| Photocatalyst	Calcination temperature (°C)	Absorption onset wavelength, λ_g (nm)	Band gap energy (eV)
Pure TiO_2		385	3.22
$0.99TiO_2$-$0.01SiO_2$		384	3.23
$0.97TiO_2$-$0.03SiO_2$	500	380	3.26
$0.95TiO_2$-$0.05SiO_2$		375	3.31
$0.93TiO_2$-$0.07SiO_2$		373	3.32
$0.97TiO_2$-$0.03SiO_2$	500	380	3.26
	600	385	3.22
	700	385	3.22
	800	388	3.20
1.25 wt.% $Pt/0.97TiO_2$-$0.03SiO_2$	500	372	3.33
0.75 wt.% Pt-0.75 wt.% $Au/0.97TiO_2$-$0.03SiO_2$	500	369	3.36

Figure 4.12 UV-visible spectrum of Eosin Y solution.

4.1.5 SEM-EDX Results

The morphology of the photocatalysts was observed by the SEM analysis. Figure 4.13 exemplifies the SEM images of the mesoporous-assembled $0.97TiO_2$-$0.03SiO_2$ mixed oxide photocatalysts calcined at 500 °C without and with 1.25 wt.% Pt and bimetallic 0.75 wt.% Pt-0.75 wt.% Au loadings. The images clearly reveal the presence of agglomerated clusters formed by an aggregation of several uniform-sized photocatalyst nanoparticles. Therefore, the nanoparticle aggregation plausibly led to the formation of mesoporous-assembled structure in the synthesized photocatalysts. The elemental distributions on the 1.25 wt.% Pt-loaded and 0.75wt.% Pt-0.75wt.% Au-loaded $0.97TiO_2$-$0.03SiO_2$ mixed oxide photocatalysts calcined at 500 °C were also examined by using the EDX analysis, as shown in Figures 4.14 and 4.15, respectively. The existence of dots in the elemental mappings of all investigated species (Ti, Si, O, Pt, and Au) indicates that all the elements in the Pt-loaded and Pt-Au-loaded $0.97TiO_2$-$0.03SiO_2$ mixed oxides were well dispersed throughout the bulk photocatalysts. These results confirmed the high dispersion state

of the deposited Pt and Pt-Au particles on the mixed oxide photocatalyst prepared by the PCD method.
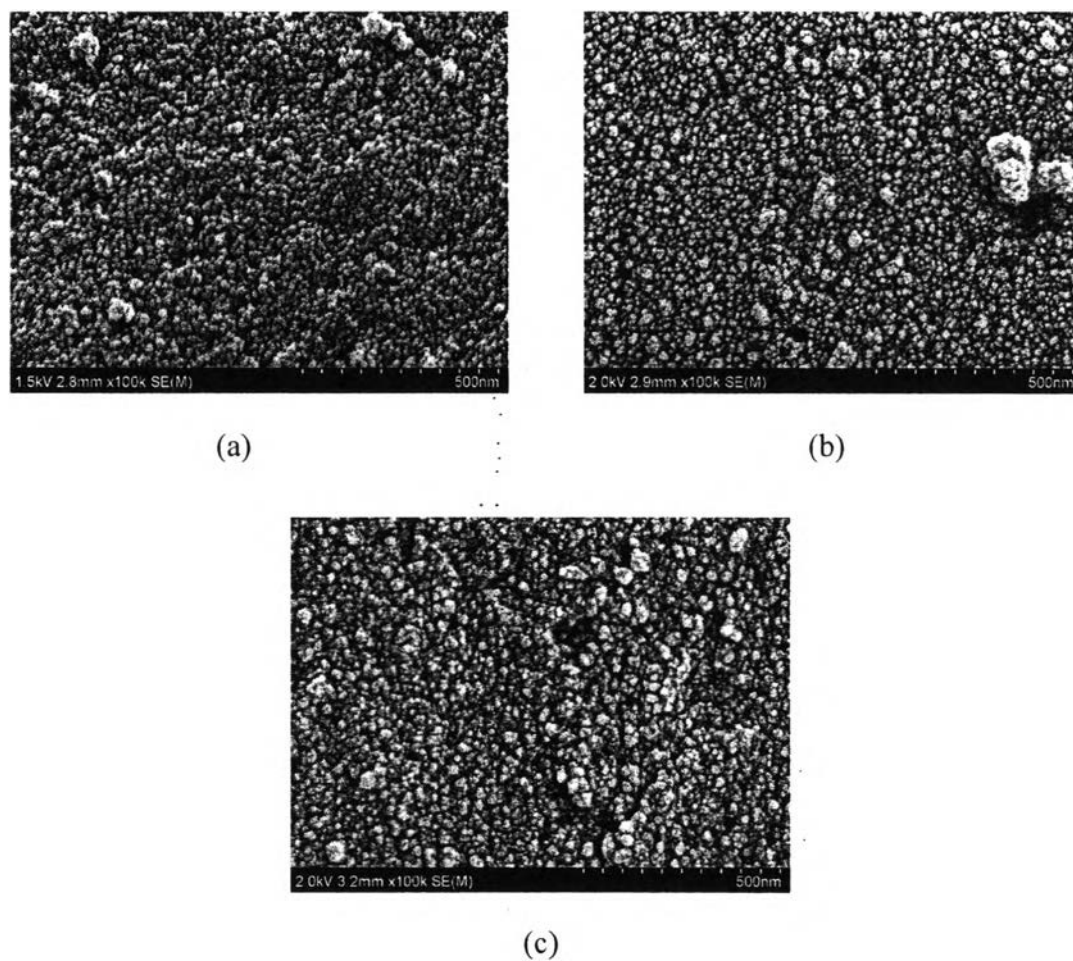

(a)

(b)

(c)

Figure 4.13 SEM images of the synthesized mesoporous-assembled photocatalysts calcined at 500 °C: (a) $0.97TiO_2$-$0.03SiO_2$ mixed oxide, (b) 1.25 wt.% Pt-loaded $0.97TiO_2$-$0.03SiO_2$ mixed oxide, and (c) 0.75 wt.% Pt-0.75 wt.% Au-loaded $0.97TiO_2$-$0.03SiO_2$ mixed oxide.
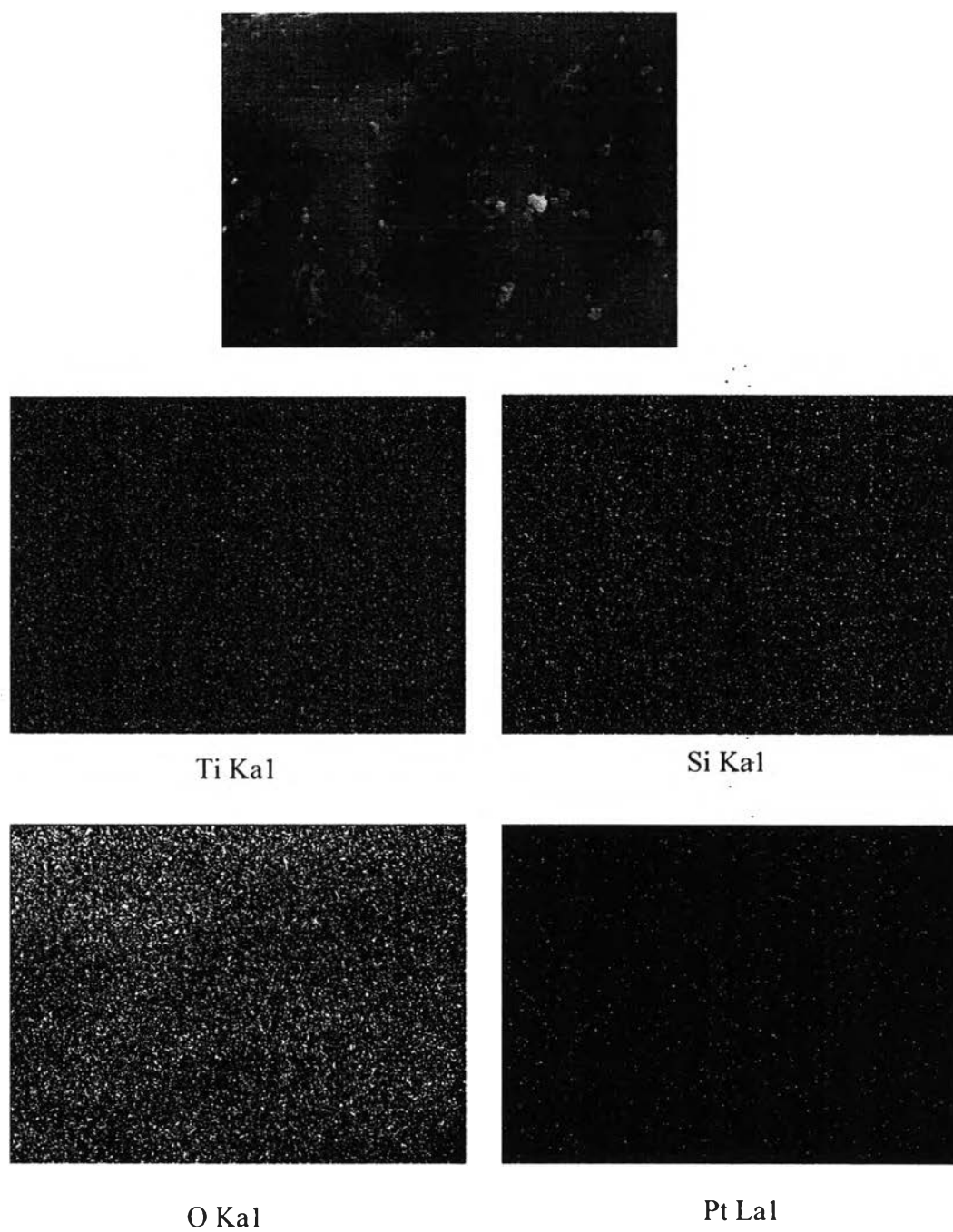
Ti Kal

Si Kal

O Kal

Pt Lal

Figure 4.14 SEM image and EDX area mappings of the synthesized 1.25 wt.% Pt-loaded mesoporous-assembled $0.97TiO_2$-$0.03SiO_2$ mixed oxide photocatalyst calcined at 500 °C.

Ti Kα1

Si Kα1

O Kα1

Pt Lα1

Au Lα1

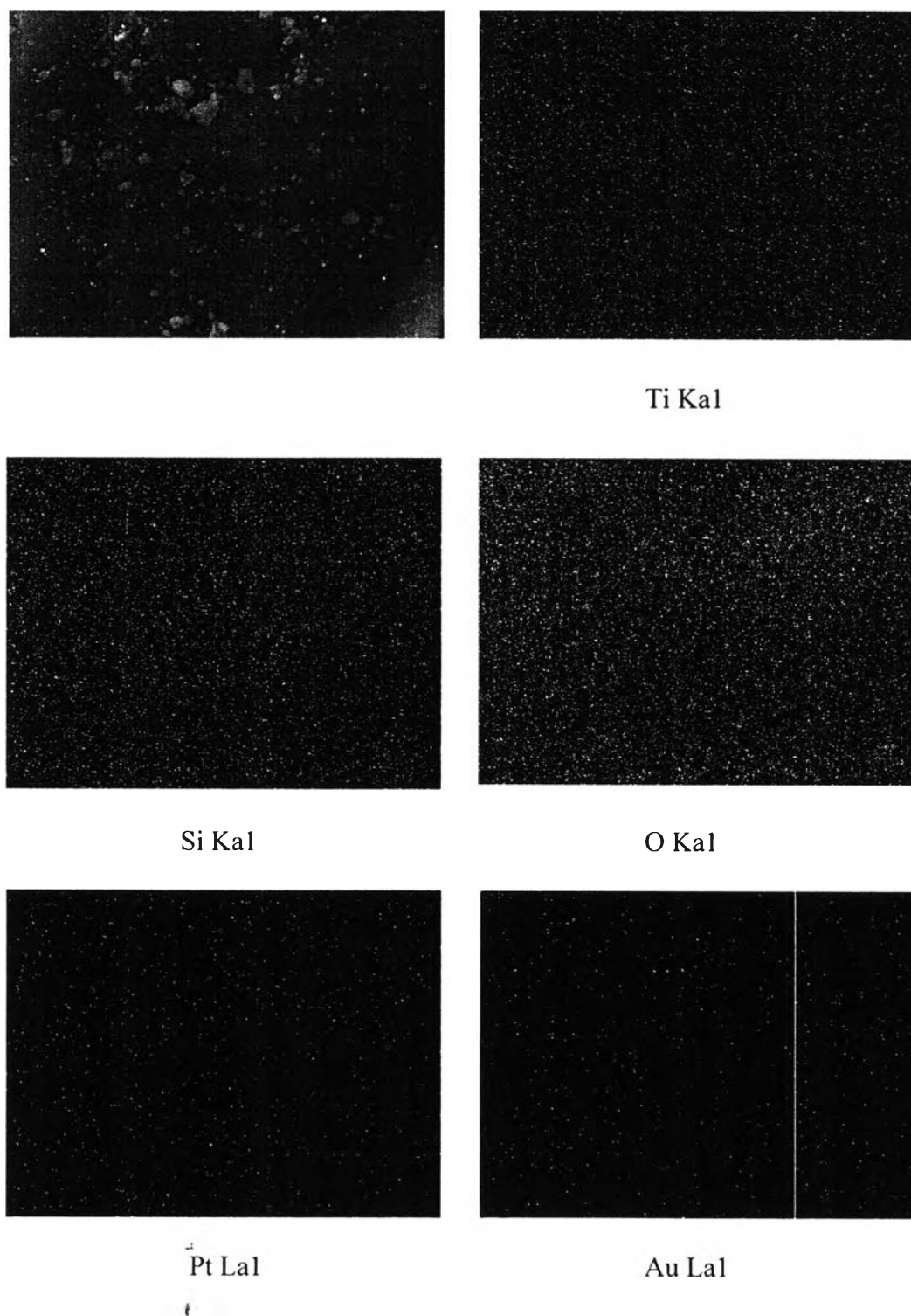**Figure 4.15** SEM image and EDX area mappings of the synthesized 0.75 wt.% Pt-0.75 wt.% Au-loaded mesoporous-assembled $0.97TiO_2$-$0.03SiO_2$ mixed oxide photocatalyst calcined at 500 °C.

4.1.6 TEM-EDX Results

The TEM analysis was performed in order to obtain insight information about the particle sizes of TiO_2-SiO_2 mixed oxide, Pt, and Pt-Au nanoparticles. Figure 4.16 shows the exemplified TEM images of the synthesized mesoporous-assembled pure TiO_2 and $0.97TiO_2$-$0.03SiO_2$ mixed oxide photocatalysts calcined at 500 °C. The TEM images reveal the formation of aggregated photocatalyst nanoparticles. The average particle sizes of the pure TiO_2 and $0.97TiO_2$-$0.03SiO_2$ mixed oxide photocatalysts were in the range of 8-15 and 5-10 nm, respectively, where the observed particle sizes are in good accordance with the crystallite sizes estimated from the XRD analysis. The smaller particle size of the $0.97TiO_2$-$0.03SiO_2$ mixed oxide can be attributed to increases in the thermal stability and the resistance to sintering caused by the incorporated SiO_2, as mentioned above. Figure 4.17 shows the TEM image and EDX point mapping of the synthesized 1.25 wt.% Pt-loaded mesoporous-assembled $0.97TiO_2$-$0.03SiO_2$ mixed oxide photocatalyst. The loaded Pt nanoparticles could be clearly seen as dark patches on the mixed oxide surface due to their high electron density, as confirmed by the EDX mapping. The average particle size of the loaded Pt nanoparticles was in the range of 5-10 nm. In addition, Figure 4.18 shows the TEM image and EDX point mapping of the synthesized bimetallic 0.75 wt.% Pt-0.75 wt.% Au-loaded mesoporous-assembled $0.97TiO_2$-$0.03SiO_2$ mixed oxide photocatalyst. It was found that even though the loaded Pt and Au tended to agglomerate and exist together as bimetallic nanoparticles, the average particle size of the loaded Pt-Au nanoparticles was very small in the range of 20-40 nm. Besides, they still exhibited very acceptably high dispersion on the mixed oxide photocatalyst, as shown in the next section.

(a)

(b)
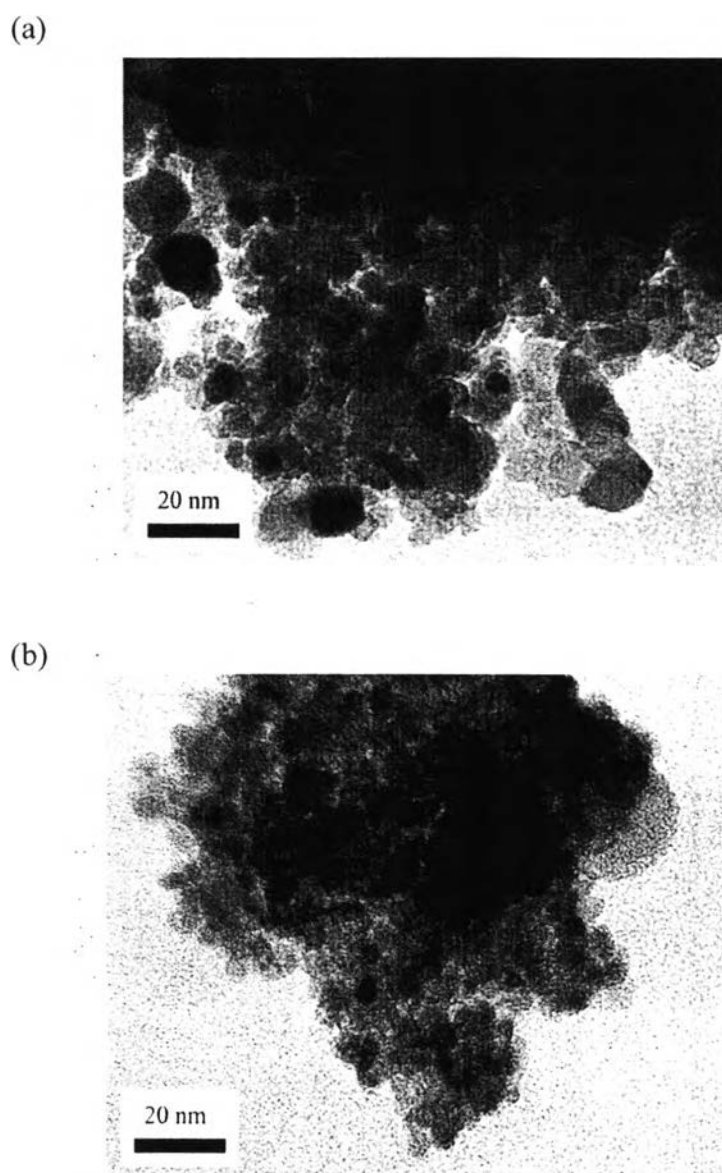
Figure 4.16 TEM images of the synthesized mesoporous-assembled photocatalysts calcined at 500 °C: (a) pure TiO_2 and (b) $0.97TiO_2$-$0.03SiO_2$ mixed oxide.

Figure 4.17 TEM image and EDX point mapping of the synthesized 1.25 wt.% Pt-loaded mesoporous-assembled $0.97TiO_2$-$0.03SiO_2$ mixed oxide photocatalyst calcined at 500 °C.

Figure 4.18 TEM image and EDX point mapping of the synthesized 0.75 wt.% Pt-0.75 wt.% Au-loaded mesoporous-assembled $0.97TiO_2$-$0.03SiO_2$ mixed oxide photocatalyst calcined at 500 °C.

4.1.7 Hydrogen Chemisorption Results

The metal dispersion was determined by hydrogen chemisorption analysis. The Pt dispersion results over the synthesized Pt-loaded mesoporous-assembled $0.97TiO_2$-$0.03SiO_2$ mixed oxide photocatalysts are given in Table 4.9. The results reveal that the Pt dispersion increased with increasing Pt loading to reach a maximum value at the 1.25 wt.% Pt, and after that it decreased with further increasing Pt loading, probably due to the Pt nanoparticle agglomeration at very high Pt loading. The maximum Pt dispersion of 82.71% at the 1.25 wt.% Pt loading is quite high, indicating that the PCD method employed for the Pt loading is very efficient to be used to achieve high metal dispersion under an appropriate metal loading range. Moreover, Table 4.10 presents the metal dispersion results over the synthesized bimetallic Pt-Au-loaded mesoporous-assembled $0.97TiO_2$-$0.03SiO_2$ mixed oxide photocatalysts. The trend of metal dispersion in the case of bimetallic Pt-Au loading was similar to the Pt dispersion in the case of monometallic Pt loading. The maximum metal dispersion of 76.2% was observed at the 0.75 wt.% Pt-0.75 wt.% Au loading.

Table 4.9 Pt dispersion results over the Pt-loaded mesoporous-assembled $0.97TiO_2$-$0.03SiO_2$ mixed oxide photocatalysts calcined at 500 °C

Pt loading (wt.%)	Pt dispersion (%)
0.5	53.86
0.75	58.75
1	67.86
1.25	82.71
1.5	66.35

Table 4.10 Metal dispersion results over the bimetallic Pt-Au-loaded mesoporous-assembled $0.97TiO_2$-$0.03SiO_2$ mixed oxide photocatalysts calcined at 500 °C

Pt loading (wt.%)	Au loading (wt.%)	Metal dispersion (%)
1.5	0	66.35
1.25	0.25	68.12
1	0.5	71.61
0.75	0.75	76.92
0.5	1	35.68
0.25	1.25	17.40
0	1.5	13.62

4.2 Photocatalytic Hydrogen Production Activity

In this research, the photocatalytic activity of the synthesized mesoporous-assembled TiO_2-SiO_2 mixed oxide photocatalysts with different TiO_2-to-SiO_2 molar ratios calcined at various temperatures without and with metal loadings was investigated for the sensitized hydrogen production from a diethanolamine (DEA) aqueous solution containing Eosin Y sensitizer (E.Y.) under visible light irradiation.

4.2.1 Effect of TiO_2-to-SiO_2 Molar Ratio in Mixed Oxide Photocatalysts

In this photocatalytic reaction, a 0.2 g of different types of the mesoporous-assembled TiO_2-SiO_2 mixed oxide photocatalysts was suspended in 150 ml of 15 vol.% DEA aqueous solution (22.5 ml DEA and 127.5 ml distilled water) containing dissolved 0.1 mM E.Y. at room temperature, which was used as the photocatalytic reaction mixture. The results of specific hydrogen production rate of the mesoporous-assembled TiO_2-SiO_2 mixed oxide photocatalysts with various TiO_2-to-SiO_2 molar ratios varying from 100:0 to 93:7 and calcined at various temperatures

are shown in Figure 4.19. It can be clearly observed that the specific hydrogen production rate reached a maximum value at a TiO_2-to-SiO_2 molar ratio of 97:3 (3 mol% SiO_2 content) and a calcination temperature of 500 °C. According to the specific surface area analysis (Table 4.2), the addition of SiO_2 with an appropriate amount increased the specific surface area of the photocatalyst, consequently resulting in more available active sites on the photocatalyst surface. The obvious decrease in the photocatalytic activity at higher SiO_2 contents is possibly because the SiO_2 itself has a very large band gap energy of approximately 8–8.9 eV (Nguyen *et al.*, 2003). Therefore, too much SiO_2 incorporation led to an undesirably large increase in the band gap energy of the TiO_2-SiO_2 mixed oxide photocatalysts (Table 4.8), especially with SiO_2 contents higher than 3 mol%. In addition, this too much SiO_2 incorporation resulted in very small crystallite size of the mixed oxides (Table 4.5), which possibly facilitated carrier charge recombination at the surface traps. Hence, the SiO_2 incorporation higher than 3 mol% was found to be unfavorable in achieving high photocatalytic hydrogen production activity. Besides, the photocatalytic hydrogen production activity of the mesoporous-assembled $0.97TiO_2$-$0.03SiO_2$ mixed oxide photocatalyst calcined at 500 °C (specific hydrogen production rate of 0.27 $cm^3/h \cdot g_{cat}$) is higher than that of the commercially available P-25 TiO_2 photocatalyst (specific hydrogen production rate of 0.17 $cm^3/h \cdot g_{cat}$). From the overall results, the mesoporous-assembled $0.97TiO_2$-$0.03SiO_2$ mixed oxide photocatalyst was used for further experiments.
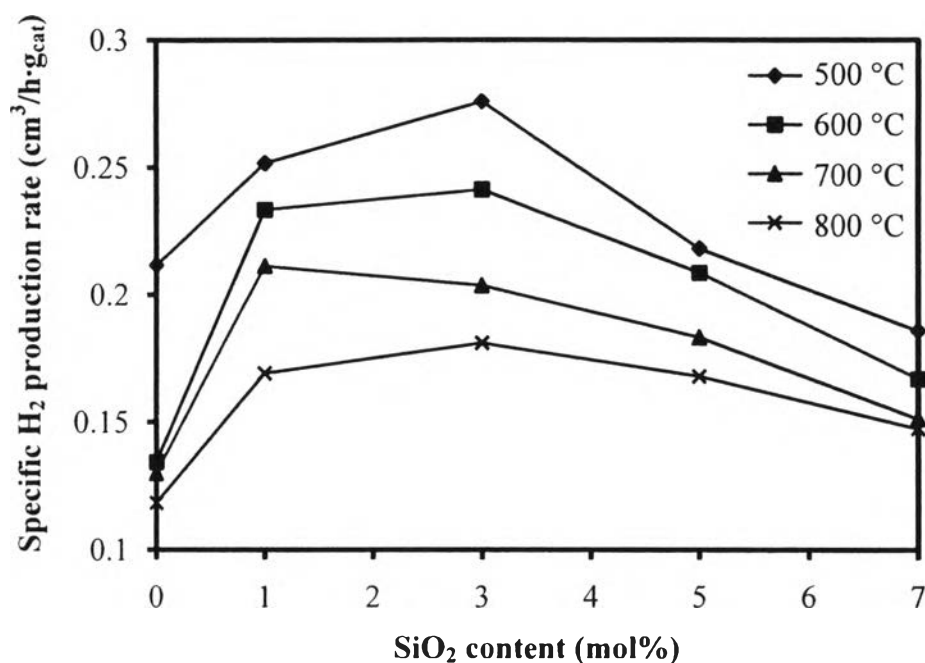
Figure 4.19 Effect of TiO_2-to-SiO_2 molar ratio in terms of SiO_2 content on specific hydrogen production rate over the mesoporous-assembled TiO_2-SiO_2 mixed oxide photocatalysts calcined at 500 °C (Photocatalyst, 0.2 g; total reaction mixture volume, 150 ml; DEA concentration, 15 vol.%; E.Y. concentration, 0.1 mM; and irradiation time, 5 h).

4.2.2 Effect of Calcination Temperature

Calcination temperature has a significant effect on the physicochemical properties and crystalline structure of a photocatalyst that definitely lead to the change in photocatalytic hydrogen production activity. Figure 4.20 shows the effect of calcination temperature on the specific hydrogen production rate over the mesoporous-assembled $0.97TiO_2$-$0.03SiO_2$ mixed oxide photocatalyst as compared to the mesoporous-assembled pure TiO_2 photocatalyst. It could be observed that the mesoporous-assembled $0.97TiO_2$-$0.03SiO_2$ mixed oxide photocatalyst exhibited a higher photocatalytic hydrogen production activity than the mesoporous-assembled pure TiO_2 photocatalyst over the entire calcination temperature range of 500-800 °C. In case of the mesoporous-assembled $0.97TiO_2$-$0.03SiO_2$ mixed oxide photocatalyst, its photocatalytic hydrogen production activity decreased with increasing calcination temperature. The highest photocatalytic

hydrogen production activity was observed at the optimum calcination temperature of 500 °C with the specific hydrogen production rate of 0.27 $cm^3/h \cdot g_{cat}$. The lower photocatalytic activity with the increase in calcination temperature is mainly because of a large decrease in the specific surface area (Table 4.1). In addition, a significant increase in the crystallite size was observed when increasing calcination temperature (Table 4.5), resulting in a higher probability of charge carrier recombination at the bulk traps. This suggest that a good control of crystallite size is required in order to prevent any charge carrier recombinations. In case of the mesoporous-assembled pure TiO_2 photocatalyst, the highest photocatalytic hydrogen production activity was also observed at the optimum calcination temperature of 500 °C with the specific hydrogen production rate of 0.21 $cm^3/h \cdot g_{cat}$, which was lower than that of the $0.97TiO_2$-$0.03SiO_2$ mixed oxide photocatalyst. Apart from the similar reasons of the negative effects of the dramatic decrease in specific surface area and the increase in crystallite size, the pure TiO_2 photocatalyst also underwent the anatase-to-rutile phase transformation starting at the calcination temperature of 600 °C (Figure 4.6(a)). It can be implied that the presence of a greater extent of rutile phase also exerts a negative effect on the photocatalytic activity. Since the rutile phase has a lower flat band potential as compared to NHE potential (H^+/H_2 level) than the anatase phase, this leads to a smaller driving force of the rutile TiO_2 for water reduction to produce hydrogen than the anatase TiO_2.
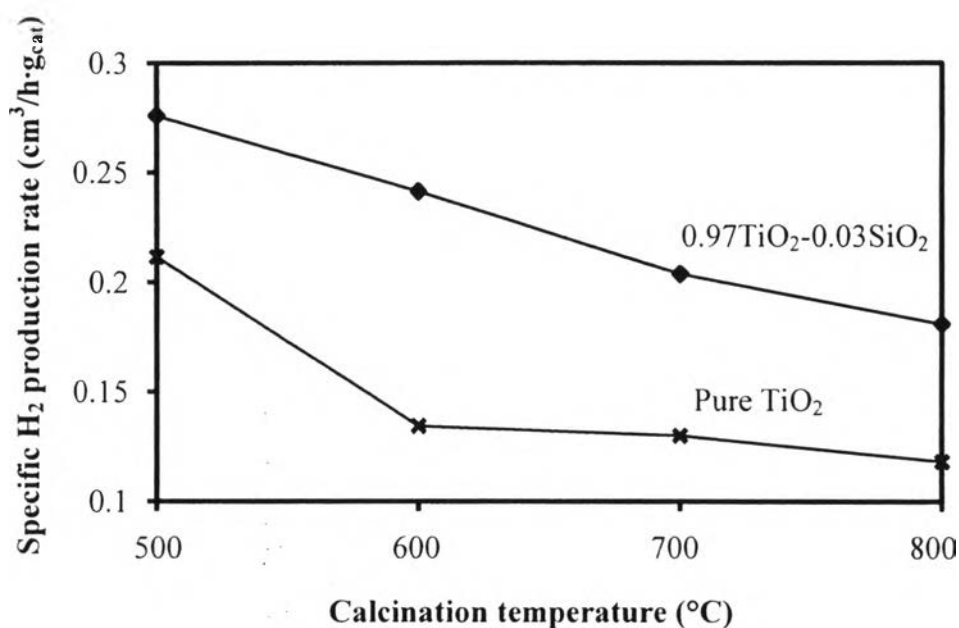
Specific H$_2$ production rate (cm^3/h·g$_{cat}$)

0.3

0.25

0.2

0.15

0.1

0.97TiO$_2$-0.03SiO$_2$

Pure TiO$_2$

500   600   700   800

Calcination temperature (°C)

Figure 4.20 Effect of calcination temperature on specific hydrogen production rate over the mesoporous-assembled pure TiO$_2$ and 0.97TiO$_2$-0.03SiO$_2$ mixed oxide photocatalysts (Photocatalyst, 0.2 g; total reaction mixture volume, 150 ml; DEA concentration, 15 vol.%; E.Y. concentration, 0.1 mM; and irradiation time, 5 h).

4.2.3 Effect of Pt- and Bimetallic Pt-Au Loadings

Noble metals are normally used to load on a photocatalyst surface to solve the problem of the charge carrier recombination that can negatively affect the photocatalytic activity. The most active metal for photocatalytic enhancement has been reported to be Pt, which can produce the highest Schottky barrier among the metals that facilitate the electron capture for further photocatalytic reaction (Vorontsov *et al.*, 1999). Figure 4.21 shows the specific hydrogen production rate of the Pt-loaded mesoporous-assembled 0.97TiO$_2$-0.03SiO$_2$ mixed oxide photocatalysts calcined at 500 °C with various Pt loadings prepared by the PCD method. In overall, it can be clearly seen that the Pt loading had a positive effect on the enhancement of the photocatalytic hydrogen production activity of the mesoporous-assembled 0.97TiO$_2$-0.03SiO$_2$ mixed oxide photocatalyst. The specific hydrogen production rate increased with increasing Pt loading and reached an optimum value before decreasing when the Pt loading was higher than 1.25 wt. %. Therefore, these results imply that the Pt loading of 1.25 wt.% was the most suitable Pt content for the

investigated $0.97TiO_2$-$0.03SiO_2$ mixed oxide photocatalyst. Even though the specific surface areas of the Pt-loaded $0.97TiO_2$-$0.03SiO_2$ mixed oxide photocatalysts moderately decreased while their crystallite sizes remained almost unchanged with varying Pt loading, as shown in Tables 4.3 and 4.6, the increase in the specific hydrogen production rate with increasing Pt loading from 0 to 1.25 wt.% can be explained in that the loaded Pt nanoparticles could enhance the photocatalytic reaction by promoting the charge carrier separation and serving as the active hydrogen production sites. It can be seen from Figure 4.21 that the specific hydrogen production rate of the 1.25 wt.% Pt-loaded $0.97TiO_2$-$0.03SiO_2$ mixed oxide photocatalyst reached the value of 1.63 $cm^3/h \cdot g_{cat}$, which was significantly enhanced by 490 % as compared to the unloaded $0.97TiO_2$-$0.03SiO_2$ mixed oxide photocatalyst. After the Pt loading exceeded such critical limit of 1.25 wt.% to be 1.5 wt.% Pt, some of them inevitably act as the electron-oxidized sensitizer recombination centers that could negatively lead to a decrease in the photocatalytic activity, resulting in decreasing specific hydrogen production rate (Zou et $al.$, 2007). These photocatalytic activity results agree well with the Pt dispersion results (Table 4.9), where the Pt dispersion increased with increasing Pt loading to 1.25 wt.% and then decreased with further increasing Pt loading to 1.5 wt.%. Hence, the Pt dispersion is another critical parameter in determining the photocatalytic activity. Since the high Pt loading of 1.5 wt.% decreased the photocatalytic activity, this high 1.5 wt.% loading was used to investigate the effect of bimetallic Pt-Au loading (dilution of Pt by Au) on improving the photocatalytic activity of the $0.97TiO_2$-$0.03SiO_2$ mixed oxide. In particular, supported bimetallic Pt-Au nanoparticles are of fundamental interest and importance. Since Au is one of only two transition metals more electronegative than Pt, the incorporation of Au into Pt nanoparticles may have unique effects on photocatalysis (Bethany et $al.$, 2007). Figure 4.22 shows the specific hydrogen production rate of the Pt-Au-loaded mesoporous-assembled $0.97TiO_2$-$0.03SiO_2$ mixed oxide photocatalysts. The total bimetallic metal loading was maintained at 1.5 wt.%, whereas the Pt loading decreased from 1.5 to 0 wt.% while the Au loading conversely increased from 0 to 1.5 wt.%. It was found that when the Pt loading gradually decreased, the specific hydrogen production rate increased until reaching a maximum value at the 0.75 wt.% Pt-0.75 wt.% Au loading (specific hydrogen

production rate of 1.54 cm^3/h·g$_{cat}$), indicating an improvement of the specific hydrogen production rate as compared to the 1.5 wt.% Pt loading. However, the further decrease in Pt loading to obtain the Au-rich bimetallic loading (Au loading higher than 0.75 wt.%) negatively affected the photocatalytic activity. When considering the physicochemical properties of the bimetallic Pt-Au-loaded 0.97TiO$_2$-0.03SiO$_2$ mixed oxide photocatalysts, the moderate variation in the specific surface area and the insignificant changes in the crystallize size and band gap energy seemed not to play an important role on the photocatalytic activity. In contrast, the metal dispersion results (Table 4.10) are believed to greatly influence the photocatalytic activity, where the highest metal dispersion was also observed at the 0.75 wt.% Pt-0.75 wt.% Au loading. The interactions between the two components in bimetallic Pt-Au nanoparticles with their suitable contents may also introduce a significant influence on the neighboring metal atoms as an ensemble effect of agglomerated Pt and Au nanoparticles, which leads to unique electronic and structural properties of the nanoparticles and improves photocatalytic activity of the monometallic Pt nanoparticles, as reported by Li *et al.* (2007). Hence, the bimetallic 0.75 wt.% Pt-0.75 wt.% Au loading was considered to be the optimum ratio at high metal loading for the effective photocatalytic hydrogen production in this work.
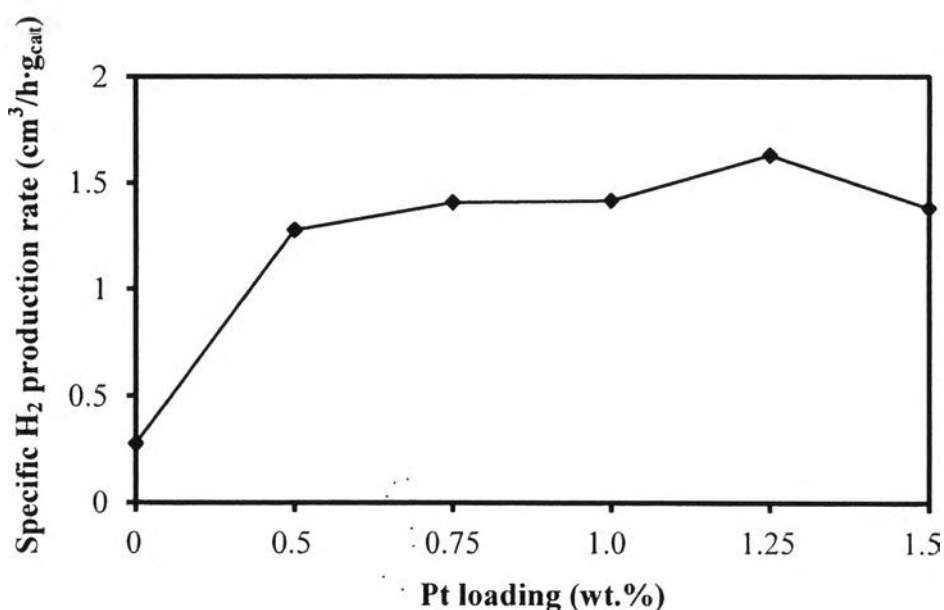
Figure 4.21 Effect of Pt loading on specific H_2 production rate over the mesoporous-assembled $0.97TiO_2$-$0.03SiO_2$ photocatalyst calcined at 500 °C (Photocatalyst, 0.2 g; total reaction mixture volume, 150 ml; DEA concentration, 15 vol.%; E.Y. concentration, 0.1 mM; irradiation time, 5 h).
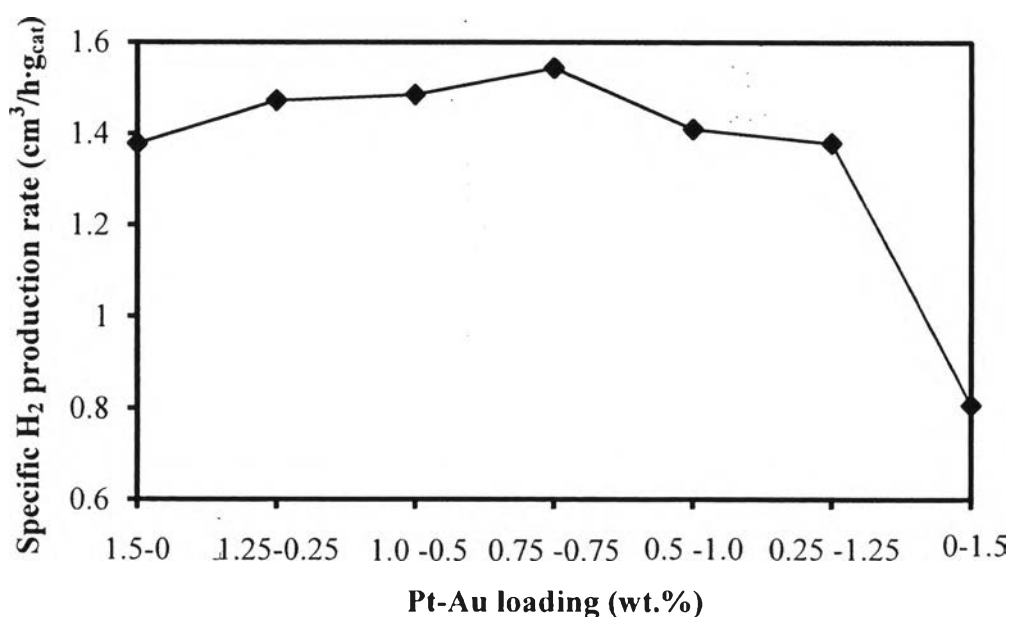

Figure 4.22 Effect of bimetallic Pt-Au loading on specific H_2 production rate over the mesoporous-assembled $0.97TiO_2$-$0.03SiO_2$ photocatalyst calcined at 500 °C (Photocatalyst, 0.2 g; total reaction mixture volume, 150 ml; DEA concentration, 15 vol.%; E.Y. concentration, 0.1 mM; irradiation time, 5 h).